

Automotive Styling Design Optimisation Based on Elliptic Fourier and Response-NSGA-II

Zhe Luo, Yu Zhong*, Xinyu Wang, Jiantao He, Xiuyun Zhai

College of Intelligent Manufacturing, Hunan University of Science and Engineering, Yongzhou 425199, China

**Corresponding author.*

Abstract:

In order to solve the problem of how to establish the mapping relationship between the optimisation objectives and design parameters in automotive styling design optimisation and the optimal solution selection of Pareto solution set, an optimisation model combining elliptic Fourier descriptor, response surface analysis and NSGA-II algorithm is proposed. Firstly, the model uses the TF-IDF algorithm to extract consumers' affective preferences for car styling design, employs elliptic Fourier descriptors to quantify car styling, and reduces dimensionality through principal component analysis techniques. Secondly, response surface analysis is used to establish the fitness function between the optimisation objective and principal components, which is applied to the NSGA-II algorithm for multi-objective optimisation to generate the Pareto solution set. Finally, response surface analysis is used again to obtain the inter-correlation between the optimisation objectives to determine the optimal emotional preference combinations, and the unique optimal solution is filtered from the Pareto solution set based on the emotional preference combinations. The method is validated by its application in the optimisation of automotive styling design, successfully overcoming the plague of multiple covariance of the least-squares method in non-linear problems, and providing a clear criterion for the NSGA-II algorithm to select the optimal solution, which ensures the uniqueness and superiority of the optimisation results.

Keywords: automotive styling, elliptic Fourier descriptor, response surface analysis, NSGA-II Algorithm, Pareto solution set

INTRODUCTION

Automotive styling design is a diversified process that integrates various factors such as art, technology and engineering [1]. Automotive product styling features can convey the brand's cultural concept, and is the most direct carrier of the brand image of automotive products[2], therefore, automotive styling design is a key link in automotive design. At present, the traditional automotive styling design process mainly includes three stages: design task analysis, artificial styling concept production and styling design scheme improvement and freezing. Among them, the artificial styling concept production stage is the core, which relies on the inspiration and experience of designers. However, this stage suffers from the uncertainty of styling concepts as well as the ambiguity and randomness of aesthetic evaluation[5,6]. In order to make automotive styling design satisfy consumers' emotional preferences and make design solutions diversified, a large number of scholars have proposed their own research theories to optimise the design of various products. Jia et al. [7] proposed a multi-objective optimal design method based on relative importance level when facing the lack of personalised demand to product parameter prediction process in product design research. Qian et al.[7] proposed a function kernel biased least squares to predict the mapping relationship between the manufacturing process and the quality of the product design, and converted the discrete series into a continuous function through functional data analysis to maintain the dynamic characteristics of the variables. dynamic properties of the variables. Wang et al.[9] For analysing the styling design of cars, GA-BP was proposed to establish a nonlinear mapping relationship between the principal component scores of car styling and the image imagery scores in order to construct the mapping relationship between consumer demand and car styling. Feng et al.[10] In solving the multi-objective optimal design problem of product reliability, an adaptive behavioural game algorithm is proposed to fit the mapping relationship between the objective function and each player's own payoff function. , which can more accurately predict the mapping relationship between the functions. Fei et al.[11] proposed a multi-strategy improvement of sparrow search algorithm, which adopts a dynamic adjustment strategy of the population in the process of applying this algorithm, limiting the number of discoveries and additions to the population, and then restricting the number of additions to the population. limiting the number of discovered and joined populations and incorporating an update strategy in the mining phase of the honeypot optimisation algorithm. Wan et al. [12] proposed an artificial fish swarm algorithm based on the response surface model, which analyses the process parameters in the injection

moulding process by using the response surface model and fits the regression equations between the process parameters and the warpage deformation, and combines the artificial fish swarm algorithm with the regression equations to search for the optimization of the process parameters and warpage deformation. Teng et al.[13] In response to the problems of convergence speed and accuracy of the grey wolf algorithm, Teng et al. For the problems of convergence speed and accuracy of the grey wolf algorithm, a grey wolf optimization algorithm combined with particle swarm optimization is proposed, which makes full use of the chaotic sequence to initialize the position of individuals to increase the diversity of the wolf packs. Zhao et al.[14] In order to solve the problem of supplier selection, a new supplier selection algorithm integrating the advantages of genetic algorithm and ant colony algorithm is proposed, which combines the evolutionary effect of the genetic algorithm and the synergistic effect of the ant colony algorithm to improve the algorithm's efficiency and effectiveness. The method combines the evolutionary effect of the genetic algorithm and the synergistic effect of the ant colony algorithm to improve the efficiency and accuracy of the algorithm.

However, there are certain shortcomings in the existing methods for optimising automotive styling improvements. Firstly, point coordinates are used in the quantification process of automotive styling contours, and the traditional point coordinate quantification of automotive styling contours has defects in the accuracy of shape analysis, especially when dealing with complex elliptical contours, the point coordinate representation will face numerical instability under the requirement of high accuracy [15]. Secondly, the above optimization methods can easily ignore the correlation between the optimization objectives when optimizing the vehicle styling design, leading to the mapping relationship between the optimization objectives and the parameters of the vehicle styling contour to have the problem of misfit, which finally makes the optimization results of the vehicle styling to be the local optimal solution instead of the global optimal solution.

To this end, this paper proposes an elliptic Fourier analysis combined with response surface to predict the fitness function method between the principal components and the optimisation objective (e.g. Figure 1). Elliptic Fourier analysis can represent the geometric features of an ellipse as a series of coefficients of Fourier series, which can simplify the complex closed contour into a finite-dimensional parameter space, and the method effectively solves the problem when quantifying the styling contour of a car in point coordinates. Secondly, the response surface analysis method can generate the response surface map and contour map, which visually demonstrates the interaction between variables, and can effectively establish the mapping relationship between the optimisation objectives and the parameters of the automotive styling contour, and by combining with the automotive styling optimisation model of NSGA-II, the response-NSGA-II optimisation model is constructed. Finally, the correlation between the optimisation objectives is again analysed by the response surface to determine the optimal solution, which makes the resulting optimal solution more effective in balancing the conflict between the optimisation objectives and strengthens the reliability of the optimisation results.

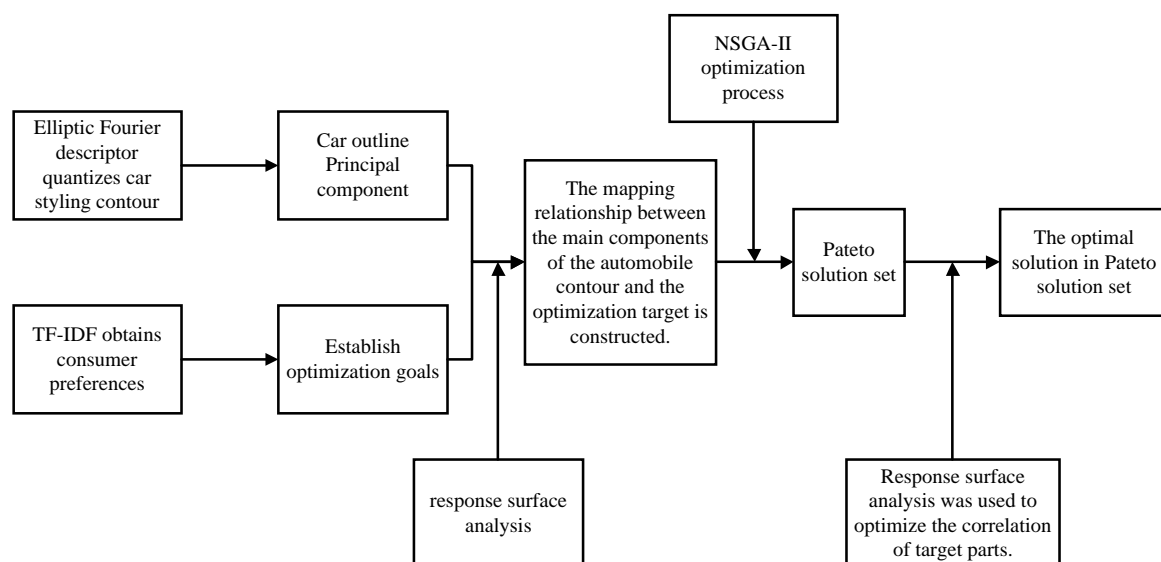


Figure 1. Elliptic fourier analysis and response surface based fitness function approach

OPTIMISATION METHODS FOR AUTOMOTIVE STYLING DESIGN

Elliptic Fourier Analysis

Elliptic Fourier analysis is a method that defines the shape feature space as a complex plane to describe two-dimensional curves, which is widely used in the fields of apparel engineering and product contour design. Compared with the conventional point coordinate numerical shape description method, the elliptic Fourier analysis method fits the contour in a more holistic way, therefore, this paper adopts the elliptic Fourier analysis to fit the car shape contour.

The elliptic Fourier analysis method has the following five main steps; firstly, pre-process the car modelling pictures; secondly, extract the boundary coordinates of the car modelling contour and transform the coordinates into a complex coordinate function, and generate a standardised sequence of new interpolated point coordinates by equidistant interpolation; then, use the elliptic Fourier series to unfold the sequence of new interpolated point coordinates, and compute the EFD coefficient matrix for the reconstructed modelling contour; finally, carry out principal component analysis of the matrix, and obtain the principal component score matrix that refines the information of the modelling contour. Finally, principal component analysis is performed on this matrix to obtain the principal component score coefficient matrix that refines the modelling contour information.

Pre-processing of car images and complex coordinate function conversion

In the pre-processing process of car images, firstly, the car images are processed into binary images and segmented; secondly, the useless background information is filtered, and then the car contour boundary features are extracted to obtain the two-dimensional contour point coordinate sequence consisting of the x, y coordinates of a discrete sampling points, which describes the styling contour of the sample product, with a certain point of the contour boundary as the starting point, and a one-week circumference around the boundary along the clockwise or counterclockwise direction, and is expressed as $(x(i), y(i))$, $i=1, 2, \dots, a-1$. The centre coordinates of this contour can be further expressed as:

$$\begin{cases} x_d \\ y_d \end{cases} = \frac{1}{a} \sum_{i=0}^{a-1} \begin{cases} x(i) \\ y(i) \end{cases} \quad (1)$$

For the purpose of subsequent elliptic Fourier transforms, a complex functional relationship is used to represent the 2D contour coordinate sequence as

$$z(i) = x(i) + jy(i) \quad (2)$$

After removing the eccentricity it is

$$z(i) = [x(i) - x_d] + j[y(i) - y_d] \quad (3)$$

Elliptic Fourier descriptor calculations

In order to standardise the different sample data points, the isometric principle is used to standardise the interpolation under the complex coordinate system, and the new interpolated point data sequence $z(v)$ can be expressed as

$$z(v) = z(m) + \frac{L_v - L_m}{L_{m+1} - L_m} [z(m+1) - z(m)] \quad (4)$$

Where: v is the new interpolated point sequence, m is the point sequence; L is the 2D contour perimeter.

$z(v)$ is a curve with period T , according to the nature of the Fourier series expansion of the periodic function, the projection of $z(v)$ in the real and imaginary axes of the complex plane can be used elliptic Fourier series expansion as

$$\begin{pmatrix} x(t) \\ y(t) \end{pmatrix} = \frac{1}{2} \begin{pmatrix} a_{x0} \\ a_{y0} \end{pmatrix} + \sum_{n=1}^N \begin{pmatrix} a_{xn} b_{xn} \\ a_{yn} b_{yn} \end{pmatrix} \begin{pmatrix} \cos\left(\frac{2n\pi t}{T}\right) \\ \sin\left(\frac{2n\pi t}{T}\right) \end{pmatrix} \quad (5)$$

Where: $\frac{a_{x0}}{2}$ is the horizontal coordinate of the contour centre point, $\frac{a_{y0}}{2}$ is the vertical coordinate of the contour centre point, n is the harmonic frequency, N is the maximum harmonic frequency and t is the arc length parameter. The above new interpolated point coordinate functions are obtained by the Riemann summation

method to obtain the four approximate elliptic Fourier coefficients of their trigonometric functions a_{xn} , b_{xn} , a_{yn} , b_{yn} :

$$\begin{pmatrix} a_{xn} \\ b_{xn} \\ a_{yn} \\ b_{yn} \end{pmatrix} = \frac{2}{A} \sum_{i=1}^A \begin{pmatrix} x_i \\ x_i \\ y_i \\ y_i \end{pmatrix} \begin{pmatrix} \cos\left(\frac{2ni\pi}{A}\right) \\ \sin\left(\frac{2ni\pi}{A}\right) \\ \cos\left(\frac{2ni\pi}{A}\right) \\ \sin\left(\frac{2ni\pi}{A}\right) \end{pmatrix} \quad (6)$$

$$G = \begin{bmatrix} a_{x1} & b_{x1} & a_{y1} & b_{y1} \\ \vdots & \vdots & \vdots & \vdots \\ a_{xn} & b_{xn} & a_{yn} & b_{yn} \end{bmatrix} \quad (7)$$

where G is the matrix of EFD coefficients, and the frequency of elliptic harmonics with four-dimensional parameters n is adjusted to approximate the contour curve of the object. Different values of n , will lead to changes in the fitting effect of the contour curve. Specifically, low-frequency harmonics affect the overall characteristics of the contour, while high-frequency harmonics affect the local details of the contour.

Principal component analysis

Principal Component Analysis (PCA) is an effective method for downscaling multiple correlated original variables into a small number of uncorrelated new variables[16]. This method maximises the retention of information about the original variables and simplifies and reveals the intrinsic connections between the data of the original variables. In the specific process of principal component analysis, firstly, the stylistic profile of the overall sample is unfolded and described using the elliptic Fourier method, and the matrix G is generated; then, by applying the PCA technique, the matrix G is downscaled to m dimensions to satisfy a certain predefined cumulative variance contribution ratio of the principal components; ultimately, a matrix of scores related to the principal components of the overall sample can be obtained Z .

$$Z = \begin{bmatrix} Z_{11} \cdots Z_{1p} \\ \vdots \\ Z_{q1} \cdots Z_{qp} \end{bmatrix} \quad (8)$$

Where: q is the sample sequence and p is the principal component sequence number.

Optimisation Model for Response-NSGA-II

Response surface methodology is a method of fitting the relationship between the actual design variables and the response using simple expressions (usually low order polynomials)[17]. However, usually the relationship between the design variable and the response to be fitted is unknown, so based on the design of the experiment and numerical analysis, sampling is performed over the range of the independent variables to find a suitable approximation to approximately fit the relationship between the independent variables and the actual function. This approach can significantly reduce the computational time required to construct the approximation model by obtaining a fairly accurate approximation of the relationship in the design space with a small number of samples and using a simple polynomial expression. A second-order response surface model is used as an example in this paper.

$$\tilde{y} = \beta_0 + \sum_{i=1}^t \beta_i x_i + \sum_{i=1}^t \beta_{ii} x_i^2 + \sum_{i=1}^t \sum_{i < j} \beta_{ij} x_i x_j \quad (9)$$

Where: x_i ($i=1, 2, \dots, t$) denotes the i th dependent variable, \tilde{y} denotes the response surface fitting function, $\beta_0, \beta_i, \beta_{ii}, \beta_{ij}$ denotes the coefficients to be determined by the least squares method, and the number of response surface experiments constructed in this paper cannot be less than the number of coefficients to be determined.

The accuracy of the established response surface model is evaluated. The accuracy metric parameters of the response surface in this paper are R^2 and the modified complex correlation coefficient R_{adj}^2 , which are calculated as follows:

$$Q_z = \sum_{i=1}^q (y_i - \bar{y})^2 \quad (10)$$

$$Q_c = \sum_{i=1}^q (y_i - \tilde{y}_i)^2 \quad (11)$$

$$Q_h = \sum_{i=1}^q (\tilde{y}_i - \bar{y})^2 \quad (12)$$

$$R^2 = 1 - \frac{Q_c}{Q_z} \quad (13)$$

$$R_{adj}^2 = \frac{Q_c/q - q_v - 1}{Q_z/q} \quad (14)$$

Where: Q_z is the sum of squares of the total deviations of the sampling points, Q_c is the sum of squares of the residuals, Q_h is the sum of squares of the regression deviations; y_i is the sampling value of the i th sample point, \tilde{y}_i is the approximation value of the i th sample point; q is the number of sample points, q_v is the degree of freedom of Q_h .

In this paper the response surface is fitted with better accuracy when R^2 and R_{adj}^2 take larger values.

NSGA-II (Non dominated sorting genetic algorithm -II) is an improvement of the initial multi-objective genetic algorithm, which is one of the important methods for solving multi-objective optimisation problems[18]. Compared with the traditional NSGA, NSGA-II shows obvious advantages in reducing the computational complexity. It overcomes the limitation of artificially specified sharing parameters and promotes the uniform distribution of samples across the entire Pareto domain by introducing the crowding degree, which ensures the diversity of samples. By introducing an elite strategy and expanding the sampling space, NSGA-II promotes competition between parents and offspring to form the next generation, which helps retain the best individuals of the previous generation. Meanwhile, by storing the sample individuals hierarchically, NSGA-II reduces the loss of the optimal individuals and improves the overall samples, greatly optimising the accuracy of the algorithm [19].

The Response-NSGA-II method proposed in this paper retains the characteristics of the original NSGA-II, and establishes the mapping relationship between each target imagery and principal components of the design solution by incorporating response surface analysis, which is mainly divided into the following steps:

Step 1: Initialise the population $P_t(t=0)$.

Initialise a parent population of size $NP_t(t=0)$. Each time a random chromosome is generated, it needs to be compared with all previously generated individuals. If the chromosome is different from the existing individuals, it is included in the initial population; if it is the same, it is discarded to ensure population diversity.

Step 2: Grade separation and congestion calculation.

The population was ranked in the non-dominance hierarchy, with higher ranks being associated with higher individual fitness. Individual fitness in the same non-dominated rank was measured using the crowding distance. Individual crowding is calculated by making the crowding distance of individuals on the edge of the ranking infinite, and the crowding distance of individuals in the middle is calculated as follows: $i_d = \sum (f_j^{i+1} - f_j^{i-1}) / (f_j^{max} - f_j^{min})$, f_j^{i+1} denotes the value of the j objective function at $i+1$, f_j^{i-1} denotes the value of the j objective function at $i-1$, f_j^{max} denotes the maximum value of the j objective function, and f_j^{min} denotes the minimum value of the j objective function.

Step 3: Binary Tournament Selection of Parent Individuals.

Individuals i and j were randomly selected for non-dominated sorting rank comparison; if the ranks were unequal, the individual with the smaller sorting value was selected; if the ranks were equal, the crowding comparison was performed, and the one with the larger crowding was selected. The process is repeated and two parents are selected for the next step of cross-mutation.

Step 4: Crossover, Variation.

In the experiment a crossover was used, where the mutation produced two offspring, and the process of crossover mutation was repeated until a new population with a population size of N was produced Q_t .

Step 5: Consolidation of populations.

The parent population P_t and the offspring population Q_t were merged into a new population H_t at $2N$.

Step 6: The population H_t is subjected to non-dominated rank ordering and congestion calculation to produce a new population P_t+1 .

Identical chromosomes in the new population were removed, non-dominated solution rank ordering and crowding calculations were performed, and the more adapted N individuals were selected to form the new population P_t+1 .

Step 7: The number of cycles is determined.

Repeat steps 3-6 until the loop algebra is exceeded, ending the algorithm.

CASE STUDIES

Automobile styling design is an important factor for users to buy automobiles, and at the same time, automobiles are also typical products with diversified emotions. Therefore, the front-view profile, side-view profile and rear-view profile of the car are selected as the object of product design optimisation this time.

Determination of Vehicle Styling Optimisation Objectives Based on TF-IDF

In this paper, by adopting crawler in the car sales software in order to obtain the user's comments on the car, we obtain the user's emotional imagery of the car according to the TF-IDF algorithm. Compared with the traditional questionnaire form to obtain users' emotional imagery of car styling, TF-IDF has the characteristics of processing large amount of data and rapid calculation[21], which makes users' emotional imagery more representative.

TF denotes the frequency of occurrence of a word in the comment text. As a weight to measure the importance of a word, the value of TF determines to a great extent the probability of a word being selected as the target imagery. The formula for TF is as follows:

$$TF = \frac{n_{i,j}}{\sum_k n_{k,j}} \quad (15)$$

$n_{i,j}$ indicates the number of times the entry t_i appears in the description of the programme d_j ; $\sum_k n_{k,j}$ indicates the total number of entries for the programme d_j .

IDF is the Inverse Text Frequency, which can be obtained by dividing the total number of programme descriptions by the number of programme descriptions containing the term, and then taking the logarithm of the resulting quotient. The fewer the documents containing the entry, the larger the IDF, which indicates that the entry has a good ability to distinguish between categories. The formula is as follows:

$$IDF = \log \frac{|D|}{|\{j: t_i \in d_j\}| + 1} \quad (16)$$

where $|D|$ is the total number of programme descriptions and $|\{j: t_i \in d_j\}|$ is the number of programme descriptions containing the term t_i .

Finally, the TF-IDF is calculated as:

$$TF-IDF = TF_{i,j} \times IDF_i \quad (17)$$

Since the different descriptions of the programmes make the text of different lengths, Eq. (16) needs to be normalised and the processed Eq. is as follows:

$$TF-IDF = \frac{TF_i \times IDF_i \times \log \left(\frac{|D|}{|\{j: t_i \in d_j\}| + 1} \right)}{\sqrt{\sum_{j=1}^n (TF_i \times \log \left(\frac{|D|}{|\{j: t_i \in d_j\}| + 1} \right))^2}} \quad (18)$$

Crawling 20,000 descriptions about the scenarios in this study in the car sales platform. According to the above Eqs. 15-18, the user emotional imagery was calculated as shown in Table 1 below, and the words such as verbs, nouns, adverbs, etc., which could not reflect the user's emotional imagery, were removed from the results. The TF-IDF size was determined as the car optimisation goal for the three imagery of atmospheric, stylish and dynamic.

Table 1. Consumer emotional imagery word TF-IDF results

emotional imagery	Number of occurrences	TF	TF-IDF
atmospheric	8060	0.011	0.009
stylish	7101	0.010	0.008
lively	4113	0.006	0.006
⋮	⋮	⋮	⋮

Quantification of Vehicle Styling Parameters Based on Elliptic Fourier

In this paper, the research focuses on the front-view overall contour, side-view overall contour and rear-view contour of automobile modelling. Considering the actual engineering application, the same shape and thin line of the wheel, lights, waistline, door frame and other secondary design elements wireframe are superimposed on each silhouette to form a more complete silhouette line as the core feature of the automotive styling imagery research object. Fifty samples were obtained through the online platform of Automotive House, and nine three-view styling images of automobiles were obtained as optimisation objects after the evaluation process, as shown in Figure 2.



Figure 2. Vehicle optimisation object diagram

The sample images are preprocessed and the contour shape of the sample is extracted as the optimised product sample. Principal component analysis is performed on the optimised sample, and after testing, the contour can be fitted better when the principal component score is 5, at which time the cumulative variance contribution rate reaches 99.9% as shown in Table 2. The principal component score matrices of the three views of the optimised sample are calculated according to Eqs. (1)-(8) as shown in Tables 3-5.

Table 2. Contribution of variance of each principal component

principal component	variance contribution	Cumulative variance contribution
Principal Component 1	88.051	88.051
Principal component 2	7.831	95.882
Principal component 3	2.751	98.633
Principal Component 4	0.915	99.548
Principal Component 5	0.403	99.951

Table 3. Overall sample side view principal component score matrix

serial number	Principal Component 1	Principal component 2	Principal component 3	Principal Component 4	Principal Component 5
Sample 1	-1.829	-0.727	1.691	-0.833	0.310
Sample 2	0.034	4.500	0.193	0.374	0.289
Sample 3	-1.465	-0.704	-0.423	0.766	-0.995
Sample 4	10.256	-0.510	1.018	-0.087	-0.216
Sample 5	-1.976	0.167	-0.312	0.636	-0.743
Sample 6	-3.613	0.097	1.057	-1.368	-0.405
Sample 7	-1.196	-0.870	0.248	0.647	1.106
Sample 8	1.300	-0.208	-3.456	-0.939	0.246
Sample 9	-1.508	-1.743	-0.0156	0.804	0.4074

Table 4. Overall sample front view principal component score matrix

serial number	Principal Component 1	Principal component 2	Principal component 3	Principal Component 4	Principal Component 5
Sample 1	22.162	-1.826	0.458	-0.912	-0.198
Sample 2	6.431	4.179	0.493	7.254	0.083
Sample 3	22.385	-1.978	0.408	-0.824	-0.114
Sample 4	22.226	-1.7512	0.315	-1.015	-1.016
Sample 5	-33.127	18.559	-17.869	-0.813	-0.023
Sample 6	22.321	-1.835	0.157	-1.102	-0.260
Sample 7	22.283	-1.520	0.103	-1.452	1.528
Sample 8	-45.626	-37.492	0.734	-0.038	0.007
Sample 9	-39.055	23.664	15.202	-1.097	-0.008

Table 5. Overall sample front view principal component score matrix

serial number	Principal Component 1	Principal component 2	Principal component 3	Principal Component 4	Principal Component 5
Sample 1	1.252	-1.409	-0.475	-1.106	-0.763
Sample 2	0.265	-0.430	-1.834	0.424	-0.567
Sample 3	1.338	0.118	-0.061	-0.019	1.651
Sample 4	2.721	-0.671	1.694	-0.993	0.042
Sample 5	0.405	-0.457	1.172	2.136	-0.353
Sample 6	-5.913	-1.431	0.156	-0.144	0.375
Sample 7	1.465	0.727	-1.436	0.209	0.479
Sample 8	-2.917	2.489	0.459	-0.621	-0.380
Sample 9	1.386	1.064	0.324	0.116	-0.483

Mapping of Optimisation Objective to Principal Components Based on Response Surface Calculation

The car styling principal components 1~5 are set as the response surface experimental independent variables $X_1 \sim X_5$, the optimisation target atmospheric, fashionable, dynamic as the model response value $Y_1 \sim Y_3$. According to B-Benhkn design parameter scheme, the simulation simulation results of 46 groups of parameter scheme are obtained as shown in Table 6, due to the excessive data only in the text to show the experimental data of the side view atmospheric.

Table 6. Side view atmospheric emotional word response surface experimental data table

serial number	Principal Component 1	Principal component 2	Principal component 3	Principal Component 4	Principal Component 5	Scoring results
1	-3.613	1.3785	-3.456	-0.282	0.05	7.7
2	10.256	1.3785	-3.456	-0.282	0.05	6.5
3	-3.613	1.3785	1.691	-0.282	0.05	6.3
4	10.256	1.3785	1.691	-0.282	0.05	5.3
5	3.3215	1.3785	-0.8825	-1.368	-1	8.9
6	3.3215	1.3785	-0.8825	0.804	-1	9.1
7	3.3215	1.3785	-0.8825	-1.368	1.1	9.3
8	3.3215	1.3785	-0.8825	0.804	1.1	9.3
9	3.3215	-1.743	-3.456	-0.282	0.05	9.2
10	3.3215	4.5	-3.456	-0.282	0.05	9.6
11	3.3215	-1.743	1.691	-0.282	0.05	9.3
12	3.3215	4.5	1.691	-0.282	0.05	9.2
13	-3.613	1.3785	-0.8825	-1.368	0.05	7.3
14	10.256	1.3785	-0.8825	-1.368	0.05	5.3
15	-3.613	1.3785	-0.8825	0.804	0.05	5.5
16	10.256	1.3785	-0.8825	0.804	0.05	5.3

17	3.3215	1.3785	-3.456	-0.282	-1	5.3
18	3.3215	1.3785	1.691	-0.282	-1	5.5
19	3.3215	1.3785	-3.456	-0.282	1.1	5.5
20	3.3215	1.3785	1.691	-0.282	1.1	5.8
21	-3.613	1.3785	-0.8825	-0.282	-1	5.8
22	10.256	1.3785	-0.8825	-0.282	-1	5.8
23	-3.613	1.3785	-0.8825	-0.282	1.1	5.6
24	10.256	1.3785	-0.8825	-0.282	1.1	6.5
25	3.3215	-1.743	-0.8825	-1.368	0.05	8.5
26	3.3215	4.5	-0.8825	-1.368	0.05	8.6
27	3.3215	-1.743	-0.8825	0.804	0.05	8.8
28	3.3215	4.5	-0.8825	0.804	0.05	8.5
29	3.3215	1.3785	-0.8825	-0.282	0.05	8
30	3.3215	1.3785	-0.8825	-0.282	0.05	8
31	3.3215	1.3785	-0.8825	-0.282	0.05	8.3
32	3.3215	1.3785	-0.8825	-0.282	0.05	8
33	3.3215	1.3785	-0.8825	-0.282	0.05	8
34	3.3215	1.3785	-0.8825	-0.282	0.05	8.5
35	-3.613	1.3785	-3.456	-0.282	0.05	7.7
36	10.256	1.3785	-3.456	-0.282	0.05	6.5
37	-3.613	1.3785	1.691	-0.282	0.05	6.3
38	10.256	1.3785	1.691	-0.282	0.05	5.3
39	3.3215	1.3785	-0.8825	-1.368	-1	8.9
40	3.3215	1.3785	-0.8825	0.804	-1	9.1
41	3.3215	1.3785	-0.8825	-1.368	1.1	9.3
42	3.3215	1.3785	-0.8825	0.804	1.1	9.3
43	3.3215	-1.743	-3.456	-0.282	0.05	9.2
44	3.3215	4.5	-3.456	-0.282	0.05	9.6
45	3.3215	-1.743	1.691	-0.282	0.05	9.3
46	3.3215	4.5	1.691	-0.282	0.05	9.2

The response functions of each optimisation objective for each view resulting from the experiments performed on the data are as follows:

The results of the response surface fitting function for the side view are as follows

$$Y_1 = 9.07 - 0.019X_1 + 0.25X_2 + 0.563X_3 + 0.094X_4 + 0.1X_5 + 0.25X_1X_2 - 0.025X_1X_3 + 0.075X_1X_4 - 0.475X_2X_3 - 0.325X_2X_5 - 0.1X_3X_4 \\ + 0.2X_3X_5 + 0.85X_4X_5 - 1.37X_1^2 - 0.477X_2^2 - 0.36X_3^2 - 1.34X_4^2 - 0.544X_5^2$$

$$Y_2 = 8.13 - 0.456X_1 - 0.15X_2 - 0.15X_3 - 0.1X_4 + 0.019X_5 + 0.9X_1X_2 + 0.05X_1X_3 + 0.45X_1X_4 + 0.225X_1X_5 - 0.125X_2X_3 - 0.1X_2X_4 \\ + 0.025X_2X_5 + 0.05X_3X_4 + 0.025X_3X_5 - 0.05X_4X_5 - 2.09X_1^2 + 0.333X_2^2 - 0.267X_3^2 + 0.5X_4^2 - 0.708X_5^2$$

$$Y_3 = 7.52 - 0.631X_1 - 0.131X_2 - 0.181X_3 - 0.238X_4 + 0.169X_5 + 0.475X_1X_3 + 1.3X_1X_4 + 0.15X_1X_5 - 0.3X_2X_3 + 0.03X_2X_4 - 0.15X_2X_5 \\ - 0.05X_3X_4 - 0.15X_3X_5 - 0.4X_4X_5 - 1.38X_1^2 + 0.35X_2^2 - 0.28X_3^2 + 0.508X_4^2 - 0.433X_5^2$$

The results of the front view response surface fitting function are as follows

$$Y_1 = 8.13 + 1.28X_1 - 0.019X_2 + 0.25X_3 + 0.025X_4 + 0.05X_5 + 0.7X_1X_2 - 0.25X_1X_3 - 0.025X_1X_4 + 0.1X_2X_3 - 0.9X_2X_4 - 0.225X_2X_5 \\ - 0.2X_3X_4 + 0.55X_3X_5 + 0.475X_4X_5 - 1.37X_1^2 - 0.752X_2^2 - 0.152X_3^2 - 0.394X_4^2 - 0.627X_5^2$$

$$Y_2 = 7.7 + 1.26X_1 - 0.031X_2 + 0.306X_3 + 0.063X_4 - 0.019X_5 + 0.5X_1X_2 - 0.35X_1X_3 - 0.075X_1X_4 - 0.2X_2X_3 - 0.95X_2X_4 - 0.325X_2X_5 \\ + 0.025X_3X_4 - 0.15X_3X_5 + 0.4X_4X_5 - 0.727X_1^2 - 0.327X_2^2 - 0.314X_3^2 - 0.519X_4^2 + 0.14X_5^2$$

$$Y_3 = 7.48 + X_1 - 4.48X_2 + 4.46X_3 - 0.006X_4 + 0.044X_5 + 0.425X_1X_2 - 0.9X_1X_3 + 0.625X_1X_5 - 17.55X_2X_3 - 1.05X_2X_4 + 0.25X_2X_5 \\ + 0.275X_3X_4 - 0.1X_3X_5 - 2.36X_1^2 + 4.41X_2^2 + 4.14X_3^2 - 2.27X_4^2 - 1.41X_5^2$$

The results of the rear view response surface fitting function are as follows

$$\begin{aligned}
 Y_1 &= 8.02 + 0.169X_1 + 0.019X_2 - 0.063X_3 - 0.213X_4 - 0.15X_5 + 0.01X_1X_2 + 0.125X_1X_3 - 0.325X_1X_4 - 0.15X_1X_5 - 0.15X_2X_3 + 0.25X_2X_5 - \\
 &\quad 0.1X_3X_4 + 0.1X_3X_5 - 0.05X_4X_5 - 2.36X_1^2 - 0.18X_2^2 + 0.18X_3^2 + 0.41X_4^2 - 0.004X_5^2 \\
 Y_2 &= 7.97 + 0.06X_1 + 0.013X_2 - 0.06X_3 - 0.07X_4 + 0.07X_5 + 0.325X_1X_2 + 0.45X_1X_4 + 0.125X_2X_3 - 0.25X_2X_5 + 0.075X_3X_4 + 0.025X_4X_5 - \\
 &\quad 1.92X_1^2 - 0.479X_2^2 + 0.154X_3^2 + 0.47X_4^2 - 0.454X_5^2 \\
 Y_3 &= 8.45 + 3.47X_1 - 0.04X_2 - 3.44X_3 - 0.213X_4 + 0.1X_5 - 13.75X_1X_3 - 0.125X_1X_5 - 0.075X_2X_3 + 0.5X_2X_4 - 0.25X_2X_5 - 0.175X_3X_4 - 0.35X_3X_5 \\
 &\quad + 0.3X_4X_5
 \end{aligned}$$

Vehicle Styling Optimisation

NSGA-II described in this paper is a stochastic search algorithm that draws on the mechanisms of natural selection and natural heredity, and is able to simulate the phenomena of reproduction, crossover and gene mutation in the natural heredity process, obtain candidate solutions in each iteration, and go through iterations for many times until it obtains the optimal solution. Based on the optimisation objective and principal component mapping function in the above, the multi-objective optimisation model and model constraints are constructed:

$$F1 \quad 2 \quad 3 \quad \max \quad (19)$$

$$s.t \quad \begin{cases} & -4 < PCC_1 < 10 \\ & -2 < PCC_2 < 5 \\ & -4 < PCC_3 < 2 \end{cases} \quad (20)$$

$$s.t \quad \begin{cases} & -1.4 < PCC_4 < 0.81 \\ & -1 < PCC_5 < 1.11 \\ & -39.1 < PCQ_1 < 22.4 \\ & -37.5 < PCQ_2 < 23.7 \\ & -17.9 < PCQ_3 < 15.2 \\ & -1.45 < PCQ_4 < 7.25 \\ & -0.2 < PCQ_5 < 1.53 \end{cases} \quad (21)$$

$$s.t \quad \begin{cases} & -5.91 < PCH_1 < 2.73 \\ & -1.43 < PCH_2 < 2.49 \\ & -1.84 < PCH_3 < 1.17 \\ & -1.1 < PCH_4 < 2.14 \\ & -0.76 < PCH_5 < 1.65 \end{cases} \quad (22)$$

Where: F_{\max} is the solution of Y_1, Y_2, Y_3 ; PC is the principal component of the front-view profile of the car, PCC is the principal component of the side-view profile of the car, and PCH is the principal component of the rear-view profile of the car.

The parameter settings of NSGA-II during the optimisation process are shown in Table 7, and nine Pareto solutions are obtained, whose principal component scores are shown in Tables 8-10.

Table 7. Parameter settings of NSGA-II

parametric	Number of Pareto solutions	population size	iteration number (math.)	crossover probability	probability of mutation
numerical value	9	30	200	0.6	0.4

Table 8. Side view pareto solution principal component scores and optimisation objective scores

Pareto solution	Principal component number					Optimisation goals		
	1	2	3	4	5	atmospheric	stylish	lively
1	1.301	-0.218	-3.422	-0.910	0.238	7.3	5.4	5.5
2	1.297	-0.223	-3.420	-0.908	0.235	6.5	7	7
3	2.195	-0.125	-2.214	-0.751	0.245	3.5	8	3
4	1.521	-0.243	-.536	-0.548	0.356	5.2	7	5
5	2.221	-0.138	-1.152	-0.354	0.350	5.6	6.5	6
6	1.009	-0.289	-0.789	-0.562	0.654	5.1	6	6
7	1.231	-0.125	-1.241	-0.689	0.335	6.3	7	7

8	1.893	-0.551	-0.396	-0.854	0.663	4.2	7	5.5
9	1.735	-0.325	-0.378	-0.213	0.554	7	6.5	3.2

Table 9. Front view pareto solution principal component scores and optimisation objective scores

Pareto solution	Principal component number					Optimisation goals		
	1	2	3	4	5	atmospheric	stylish	lively
1	22.162	-1.826	0.458	-0.912	-0.198	8.3	4.5	5
2	21.159	-1.735	0.375	-0.895	-0.155	6.5	6	6
3	20.335	-1.885	0.455	-0.755	-0.193	6.5	5	7
4	21.225	-1.705	0.315	-0.625	-0.221	6.2	7	5
5	19.835	-1.688	0.305	-0.615	-0.277	6.6	6.5	6
6	18.886	-1.678	0.255	-0.589	-0.332	7.1	6	6
7	19.851	-1.532	0.184	-0.654	-0.298	7.3	5.5	5
8	18.966	-1.355	0.254	-0.832	-0.277	6.2	5.5	5.5
9	19.355	-1.533	0.248	-0.765	-0.311	7	7.5	3.2

Table 10. Front view pareto solution principal component scores and optimisation objective scores

Pareto solution	Principal component number					Optimisation goals		
	1	2	3	4	5	atmospheric	stylish	lively
1	1.311	-1.309	-0.415	-1.115	-0.651	7.7	4	6
2	0.246	-0.375	-1.755	0.433	-0.398	5.5	6	6
3	1.128	0.211	-0.054	-0.018	1.211	4.5	7	3
4	2.533	-0.633	1.633	-0.856	0.032	4.2	7	7
5	0.411	-0.542	1.195	2.001	-0.374	5	7.5	6
6	-4.322	-1.377	0.127	-0.141	0.333	5.3	6.5	6
7	1.465	0.745	-1.356	0.318	0.551	5.3	6	6
8	-2.835	2.333	0.211	-0.646	-0.371	6.2	4.5	4.5
9	1.274	1.001	0.321	0.112	-0.356	6	5.5	5.2

According to the response surface analysis of the three optimisation objectives can get the fitting function relationship between the car styling scores and the optimisation objectives; secondly, the response surface analysis can get the correlation between the two optimisation objectives, and finally get the optimal car styling design of the three views.

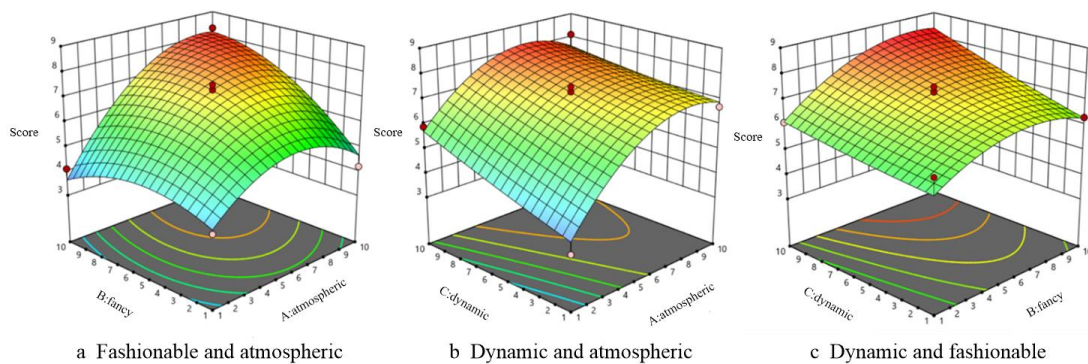


Figure 3. Two-by-two correlation response surface plots for each factor

In order to determine the optimal solution in the Pareto solution set, the correlation between the optimisation objectives is analysed in this paper as a response surface plot. The response surface analysis in Figure 3a shows that when the atmospheric score reaches the maximum value, the car styling score is also the highest. However, as the degree of fashionable increases, the car styling score decreases instead, which indicates a high degree of conflict between the two optimisation objectives of fashionable and atmospheric. Better results can be obtained when the atmospheric score is higher and the stylish score is lower. Further analysis of Figure 3b reveals that car styling is able to achieve the highest ratings when the stylish and dynamic ratings take the middle value. However, as the two optimisation objective scores are further increased, the car styling scores instead decrease. This

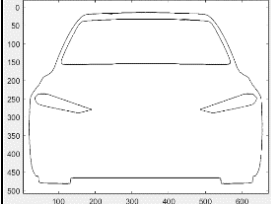
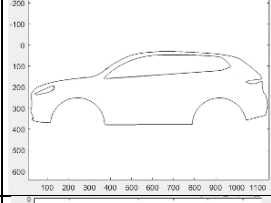
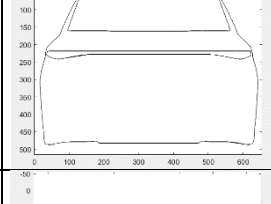
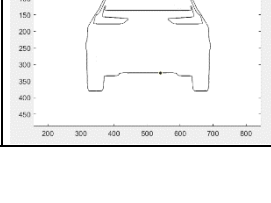
indicates a more general level of conflict between the stylish and the sporty ones, while better results can be obtained when the two ratings are taken at intermediate values. In addition, the analysis in Figure 3c shows that when the atmospheric score is taken to a larger value, a higher car styling score is obtained regardless of the value of the dynamic score. Whereas, when the atmospheric score is small, only the change in the kinetic score has less effect on the car styling score. This indicates that the degree of conflict between the atmospheric and the dynamic is minimal.

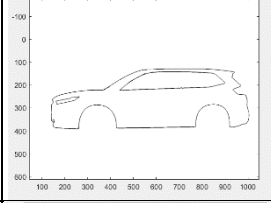
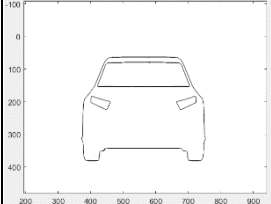
Combining the above analyses, we conclude that the car styling scores are highest when the atmospheric score takes the larger value and the stylish and dynamic scores take the middle value. Therefore, based on the scoring results in Tables 7-9, we determine that the optimal solution design in the Pareto solution set is Scheme 1.

ANALYSIS OF RESULTS

The before and after comparison of the optimisation of Scenario 1 is shown in Table 11. The analysis of the optimisation objectives shows that there is a difference in the degree of optimisation in different views for the three optimisation objectives of atmospheric, stylish and dynamic. Specifically, firstly, in the optimisation of the atmospheric optimisation objective, all three views show a higher degree of optimisation, with the side view showing the most prominent optimisation effect. Secondly, in terms of optimising this optimisation goal for fashion, the degree of optimisation is lower in all views, especially in the side view where the degree of optimisation for this optimisation goal for fashion is instead lower. This is because there is a greater degree of conflict between the optimisation objective of atmosphere and the optimisation objective of fashion, but the optimisation objective of fashion is optimised to a higher degree in the front view of the car. Finally, in terms of optimising the optimisation objective of motion, the optimisation degree of each view is average, but the optimisation degree of the optimisation objective of motion is very high in the side view. This is due to the low profile of the kinetic optimisation objective in the original image and the minimal conflict between the kinetic and atmospheric optimisation objectives.

Table 11. Comparison of car styling data and styles before and after optimisation

view	principal component data					Target Imagery Score			silhouette
	1	2	3	4	5	atmospheric	stylish	lively	
Front view optimisation	1.301	-0.218	-3.422	-0.910	0.238	7.3	5.4	5.5	
Side view optimisation	22.160	-1.826	0.458	-0.912	-0.198	8.3	5.5	5	
Rear view optimisation	1.311	-1.309	-0.415	-1.115	-0.651	7.7	5	6	
proto-anterior vision	1.023	-0.056	-2.132	-0.837	0.135	3.2	3.3	5.5	

original side view	12.160	-1.525	0.158	-0.712	-0.238	6.3	7.1	3.5	
original posterior view	1.001	-1.979	3.335	-2.115	-0.251	5.3	3.8	5.5	

CONCLUSION

In this paper, the mapping function relationship expression obtained by combining response surface analysis and elliptic Fourier analysis is used as the optimisation objective function of NSGA-II and applied to the optimisation of automotive styling design. The method takes consumer demand as the optimisation objective of automobile styling, and the optimisation results effectively improve the quality of automobile styling; secondly, the correlation between the optimisation objectives and the mapping function between the optimisation objectives and the principal components are determined by response surface analysis, which effectively avoids the problem of local area solution and the existence of large repetitions and high similarity in the solution set in NSGA-II algorithm. Although the research in this paper solves a series of problems in other algorithms, there are still some limitations. Firstly, elliptic Fourier analysis can only analyse closed contours, and there is no quantitative characterisation of non-closed contours; secondly, response surface analysis can only obtain the relationship between the conflict degree of the optimisation objectives, and cannot get the comprehensive impact between more than three optimisation objectives; finally, NSGA-II can solve the problem of local optimal solutions by improving the mapping function, but the performance of the convergence speed is general. Therefore, in the future, it is still worth exploring the unresolved issues of proposing an analytical method that can analyse the correlation of more than three optimisation objectives, and proposing algorithms that can solve the problem of local optimal solutions and improve the convergence speed of the algorithms.

ACKNOWLEDGEMENT

This work was supported by the Scientific Research Project of Hunan Provincial Education Department (Grant No.23B0757, Grant No.24B0742) and the Natural Science Foundation of Hunan Province (Grant No. 2023JJ50071) and the Scientific Research Project of Hunan University of Science And Engineering (Grant No. 24XKYZ05).

REFERENCES

- [1] Zhai L Y, Khoo L P, Zhong Z W. A dominance-based rough set approach to Kansei Engineering in product development. *Expert Systems With Applications*, 2009, 36(1): 393-402.
- [2] Hu H, Liu Y, Lu W F, et al. A quantitative aesthetic measurement method for product appearance design. *Advanced Engineering Informatics*, 2022, 53: 101644.
- [3] Kato T, Botella-Carrubi D, Ribeiro-Navarrete S. The value created by the removal of cut lines: evaluating the impact of finishing of industrial designs on purchase intention. *Journal of Consumer Behaviour*, 2023, 22(4): 942-954.]
- [4] Zhu S. Development of Visual Culture in Product Design with Application of Digital Mining Technology. *Applied Mathematics and Nonlinear Sciences*.
- [5] Zhou A, Liu H, Zhang S, et al. Evaluation and design method for product form aesthetics based on deep learning. *IEEE Access*, 2021, 9: 108992-109003.
- [6] Zong L, Wang N. A Product Modeling Design Decision Model Based on PGA Genetic Algorithm. *Mathematical Problems in Engineering*, 2022, 2022(1): 7794320.

- [7] Jia liangyue, Hao jia, Shang xiwen, et al. Lightweight design optimization of truss structure using long short-term memory network *Computer Integrated Manufacturing Systems*, 2023,29(10):3317-3330 (in chinese).
- [8] Qian Q, Li M, Xu J. Dynamic prediction of multivariate functional data based on functional kernel partial least squares. *Journal of Process Control*, 2022, 116: 273-285.
- [9] Wang Z, Liu W, Yang M, et al. A Multi-Objective Evolutionary Algorithm Model for Product Form Design Based on Improved SPEA2. *Applied Sciences*, 2019, 9(14): 2944-2959.
- [10] Feng jiazhen, Zhang jianguo, Qiu jiwei. Game algorithm for reliability multi-objective design optimization based on adaptive behaviour. *Computer Integrated Manufacturing Systems*, 2019, 25(03): 736-742 (in chinese).
- [11] Fei T, Wang H, Liu L, et al. Research on multi-strategy improved sparrow search optimisation algorithm. *Mathematical Biosciences and Engineering: MBE*, 2023, 20(9): 17220-17241.
- [12] Wan liangqi, Ouyang linhan. Kriging ensemble model based on 0-1 programming model selection strategy for reliability-based design optimisation . *Computer Integrated Manufacturing Systems*, 2022,28(07):2162-2168 (in chinese).
- [13] Teng Z, Lv J, Guo L. An improved hybrid grey wolf optimisation algorithm. *Soft Computing*, 2019, 23(15): 6617-6631.
- [14] Zhao F, Yao Z, Luan J, et al. A Novel Fused Optimization Algorithm of Genetic Algorithm and Ant Colony Optimization. *Mathematical Problems in Engineering*, 2016: 2167413.
- [15] WANG Zeng, LIU Weidong, YANG Minglang, et al. Product shape imagery design based on elliptic Fourier. *Computer Integrated Manufacturing Systems*, 2020, 26(02):481-495.
- [16] Greenacre M, Groenen P J F, Hastie T, et al. Principal component analysis. *Nature Reviews Methods Primers*, 2022, 2(1): 100.
- [17] Ockuly R A, Weese M L, Smucker B J, et al. Response surface experiments: a meta-analysis. *Chemometrics and Intelligent Laboratory Systems*, 2017, 164: 64-75.
- [18] Carles-Bou J L, Galán S F. Self-adaptive polynomial mutation in NSGA-II. *Soft Computing*, 2023, 27(23): 17711-17727.
- [19] Liu S, Tian Q, Tang C. Mobile Robot Path Planning Algorithm Based on NSGA-II. *Applied Sciences*, 2024, 14(10): 4305.
- [20] Ackaah W, Kanton A T, Osei K K. Factors influencing consumers' intentions to purchase electric vehicles in Ghana. *Transportation Letters*, 2022, 14(9): 1031-1042.
- [21] Sul S, Cho S B. Understanding people's attitudes in IoT systems using wellness probes and TF-IDF data analysis. *Multimedia Tools and Applications*, 2024: 1-20.